SLAC-PUB-8537
August 2000
BaBar-CONF-00/15
hep-ex-0008058

Measurements of Charmless Three-Body and Quasi-Two-Body *B* Decays

The BaBar Collaboration

Presented at the 30th International Conference On High-Energy Physics,
7/27/2000—8/2/2000, Osaka, Japan

Stanford Linear Accelerator Center, Stanford University, Stanford, CA 94309

Work supported by Department of Energy contract DE–AC03–76SF00515.

BABAR-CONF-00/15
SLAC-PUB-8537

Measurements of charmless three-body and quasi-two-body B decays

The *BABAR* Collaboration

August 21, 2000

Abstract

We present preliminary results of a search for several exclusive charmless hadronic B decays from electron-positron annihilation data collected by the *BABAR* detector near the $\Upsilon(4S)$ resonance. These include three-body decay modes with final states $h^{\pm}h^{\mp}h^{\pm}$ and $h^{\pm}h^{\mp}\pi^0$, and quasi-two-body decay modes with final states X^0h and $X^0K^0_S$, where $h = \pi$ or K and $X^0 = \eta'$ or ω. We find $\mathcal{B}(B^0 \to \rho^{\mp}\pi^{\pm}) = (49 \pm 13^{+6}_{-5}) \times 10^{-6}$ and $\mathcal{B}(B^+ \to \eta' K^+) = (62 \pm 18 \pm 8) \times 10^{-6}$ and present upper limits for eight other decays.

Submitted to the XXXth International Conference on High Energy Physics, Osaka, Japan.

The *BABAR* Collaboration

B. Aubert, A. Boucham, D. Boutigny, I. De Bonis, J. Favier, J.-M. Gaillard, F. Galeazzi, A. Jeremie, Y. Karyotakis, J. P. Lees, P. Robbe, V. Tisserand, K. Zachariadou

Lab de Phys. des Particules, F-74941 Annecy-le-Vieux, CEDEX, France

A. Palano

Università di Bari, Dipartimento di Fisica and INFN, I-70126 Bari, Italy

G. P. Chen, J. C. Chen, N. D. Qi, G. Rong, P. Wang, Y. S. Zhu

Institute of High Energy Physics, Beijing 100039, China

G. Eigen, P. L. Reinertsen, B. Stugu

University of Bergen, Inst. of Physics, N-5007 Bergen, Norway

B. Abbott, G. S. Abrams, A. W. Borgland, A. B. Breon, D. N. Brown, J. Button-Shafer, R. N. Cahn, A. R. Clark, Q. Fan, M. S. Gill, S. J. Gowdy, Y. Groysman, R. G. Jacobsen, R. W. Kadel, J. Kadyk, L. T. Kerth, S. Kluth, J. F. Kral, C. Leclerc, M. E. Levi, T. Liu, G. Lynch, A. B. Meyer, M. Momayezi, P. J. Oddone, A. Perazzo, M. Pripstein, N. A. Roe, A. Romosan, M. T. Ronan, V. G. Shelkov, P. Strother, A. V. Telnov, W. A. Wenzel

Lawrence Berkeley National Lab, Berkeley, CA 94720, USA

P. G. Bright-Thomas, T. J. Champion, C. M. Hawkes, A. Kirk, S. W. O'Neale, A. T. Watson, N. K. Watson

University of Birmingham, Birmingham, B15 2TT, UK

T. Deppermann, H. Koch, J. Krug, M. Kunze, B. Lewandowski, K. Peters, H. Schmuecker, M. Steinke

Ruhr Universität Bochum, Inst. f. Experimentalphysik 1, D-44780 Bochum, Germany

J. C. Andress, N. Chevalier, P. J. Clark, N. Cottingham, N. De Groot, N. Dyce, B. Foster, A. Mass, J. D. McFall, D. Wallom, F. F. Wilson

University of Bristol, Bristol BS8 lTL, UK

K. Abe, C. Hearty, T. S. Mattison, J. A. McKenna, D. Thiessen

University of British Columbia, Vancouver, BC, Canada V6T 1Z1

B. Camanzi, A. K. McKemey, J. Tinslay

Brunel University, Uxbridge, Middlesex UB8 3PH, UK

V. E. Blinov, A. D. Bukin, D. A. Bukin, A. R. Buzykaev, M. S. Dubrovin, V. B. Golubev, V. N. Ivanchenko, A. A. Korol, E. A. Kravchenko, A. P. Onuchin, A. A. Salnikov, S. I. Serednyakov, Yu. I. Skovpen, A. N. Yushkov

Budker Institute of Nuclear Physics, Siberian Branch of Russian Academy of Science, Novosibirsk 630090, Russia

A. J. Lankford, M. Mandelkern, D. P. Stoker

University of California at Irvine, Irvine, CA 92697, USA

A. Ahsan, K. Arisaka, C. Buchanan, S. Chun

University of California at Los Angeles, Los Angeles, CA 90024, USA

J. G. Branson, R. Faccini,[1] D. B. MacFarlane, Sh. Rahatlou, G. Raven, V. Sharma

University of California at San Diego, La Jolla, CA 92093, USA

C. Campagnari, B. Dahmes, P. A. Hart, N. Kuznetsova, S. L. Levy, O. Long, A. Lu, J. D. Richman, W. Verkerke, M. Witherell, S. Yellin

University of California at Santa Barbara, Santa Barbara, CA 93106, USA

J. Beringer, D. E. Dorfan, A. Eisner, A. Frey, A. A. Grillo, M. Grothe, C. A. Heusch, R. P. Johnson, W. Kroeger, W. S. Lockman, T. Pulliam, H. Sadrozinski, T. Schalk, R. E. Schmitz, B. A. Schumm, A. Seiden, M. Turri, D. C. Williams

University of California at Santa Cruz, Institute for Particle Physics, Santa Cruz, CA 95064, USA

E. Chen, G. P. Dubois-Felsmann, A. Dvoretskii, D. G. Hitlin, Yu. G. Kolomensky, S. Metzler, J. Oyang, F. C. Porter, A. Ryd, A. Samuel, M. Weaver, S. Yang, R. Y. Zhu

California Institute of Technology, Pasadena, CA 91125, USA

R. Aleksan, G. De Domenico, A. de Lesquen, S. Emery, A. Gaidot, S. F. Ganzhur, G. Hamel de Monchenault, W. Kozanecki, M. Langer, G. W. London, B. Mayer, B. Serfass, G. Vasseur, C. Yeche, M. Zito

Centre d'Etudes Nucléaires, Saclay, F-91191 Gif-sur-Yvette, France

S. Devmal, T. L. Geld, S. Jayatilleke, S. M. Jayatilleke, G. Mancinelli, B. T. Meadows, M. D. Sokoloff

University of Cincinnati, Cincinnati, OH 45221, USA

J. Blouw, J. L. Harton, M. Krishnamurthy, A. Soffer, W. H. Toki, R. J. Wilson, J. Zhang

Colorado State University, Fort Collins, CO 80523, USA

S. Fahey, W. T. Ford, F. Gaede, D. R. Johnson, A. K. Michael, U. Nauenberg, A. Olivas, H. Park, P. Rankin, J. Roy, S. Sen, J. G. Smith, D. L. Wagner

University of Colorado, Boulder, CO 80309, USA

T. Brandt, J. Brose, G. Dahlinger, M. Dickopp, R. S. Dubitzky, M. L. Kocian, R. Müller-Pfefferkorn, K. R. Schubert, R. Schwierz, B. Spaan, L. Wilden

Technische Universität Dresden, Inst. f. Kern- u. Teilchenphysik, D-01062 Dresden, Germany

L. Behr, D. Bernard, G. R. Bonneaud, F. Brochard, J. Cohen-Tanugi, S. Ferrag, E. Roussot, C. Thiebaux, G. Vasileiadis, M. Verderi

Ecole Polytechnique, Lab de Physique Nucléaire H. E., F-91128 Palaiseau, France

A. Anjomshoaa, R. Bernet, F. Di Lodovico, F. Muheim, S. Playfer, J. E. Swain

University of Edinburgh, Edinburgh EH9 3JZ, UK

C. Bozzi, S. Dittongo, M. Folegani, L. Piemontese

Università di Ferrara, Dipartimento di Fisica and INFN, I-44100 Ferrara, Italy

E. Treadwell

Florida A&M University, Tallahassee, FL 32307, USA

[1] Jointly appointed with Università di Roma La Sapienza, Dipartimento di Fisica and INFN, I-00185 Roma, Italy

R. Baldini-Ferroli, A. Calcaterra, R. de Sangro, D. Falciai, G. Finocchiaro, P. Patteri, I. M. Peruzzi,[2] M. Piccolo, A. Zallo

Laboratori Nazionali di Frascati dell'INFN, I-00044 Frascati, Italy

S. Bagnasco, A. Buzzo, R. Contri, G. Crosetti, P. Fabbricatore, S. Farinon, M. Lo Vetere, M. Macri, M. R. Monge, R. Musenich, R. Parodi, S. Passaggio, F. C. Pastore, C. Patrignani, M. G. Pia, C. Priano, E. Robutti, A. Santroni

Università di Genova, Dipartimento di Fisica and INFN, I-16146 Genova, Italy

J. Cochran, H. B. Crawley, P.-A. Fischer, J. Lamsa, W. T. Meyer, E. I. Rosenberg

Iowa State University, Ames, IA 50011-3160, USA

R. Bartoldus, T. Dignan, R. Hamilton, U. Mallik

University of Iowa, Iowa City, IA 52242, USA

C. Angelini, G. Batignani, S. Bettarini, M. Bondioli, M. Carpinelli, F. Forti, M. A. Giorgi, A. Lusiani, M. Morganti, E. Paoloni, M. Rama, G. Rizzo, F. Sandrelli, G. Simi, G. Triggiani

Università di Pisa, Scuola Normale Superiore, and INFN, I-56010 Pisa, Italy

M. Benkebil, G. Grosdidier, C. Hast, A. Hoecker, V. LePeltier, A. M. Lutz, S. Plaszczynski, M. H. Schune, S. Trincaz-Duvoid, A. Valassi, G. Wormser

LAL, F-91898 ORSAY Cedex, France

R. M. Bionta, V. Brigljević, O. Fackler, D. Fujino, D. J. Lange, M. Mugge, X. Shi, T. J. Wenaus, D. M. Wright, C. R. Wuest

Lawrence Livermore National Laboratory, Livermore, CA 94550, USA

M. Carroll, J. R. Fry, E. Gabathuler, R. Gamet, M. George, M. Kay, S. McMahon, T. R. McMahon, D. J. Payne, C. Touramanis

University of Liverpool, Liverpool L69 3BX, UK

M. L. Aspinwall, P. D. Dauncey, I. Eschrich, N. J. W. Gunawardane, R. Martin, J. A. Nash, P. Sanders, D. Smith

University of London, Imperial College, London, SW7 2BW, UK

D. E. Azzopardi, J. J. Back, P. Dixon, P. F. Harrison, P. B. Vidal, M. I. Williams

University of London, Queen Mary and Westfield College, London, E1 4NS, UK

G. Cowan, M. G. Green, A. Kurup, P. McGrath, I. Scott

University of London, Royal Holloway and Bedford New College, Egham, Surrey TW20 0EX, UK

D. Brown, C. L. Davis, Y. Li, J. Pavlovich, A. Trunov

University of Louisville, Louisville, KY 40292, USA

J. Allison, R. J. Barlow, J. T. Boyd, J. Fullwood, A. Khan, G. D. Lafferty, N. Savvas, E. T. Simopoulos, R. J. Thompson, J. H. Weatherall

University of Manchester, Manchester M13 9PL, UK

[2]Jointly appointed with Univ. di Perugia, I-06100 Perugia, Italy

C. Dallapiccola, A. Farbin, A. Jawahery, V. Lillard, J. Olsen, D. A. Roberts
University of Maryland, College Park, MD 20742, USA

B. Brau, R. Cowan, F. Taylor, R. K. Yamamoto
Massachusetts Institute of Technology, Lab for Nuclear Science, Cambridge, MA 02139, USA

G. Blaylock, K. T. Flood, S. S. Hertzbach, R. Kofler, C. S. Lin, S. Willocq, J. Wittlin
University of Massachusetts, Amherst, MA 01003, USA

P. Bloom, D. I. Britton, M. Milek, P. M. Patel, J. Trischuk
McGill University, Montreal, PQ, Canada H3A 2T8

F. Lanni, F. Palombo
Università di Milano, Dipartimento di Fisica and INFN, I-20133 Milano, Italy

J. M. Bauer, M. Booke, L. Cremaldi, R. Kroeger, J. Reidy, D. Sanders, D. J. Summers
University of Mississippi, University, MS 38677, USA

J. F. Arguin, J. P. Martin, J. Y. Nief, R. Seitz, P. Taras, A. Woch, V. Zacek
Université de Montreal, Lab. Rene J. A. Levesque, Montreal, QC, Canada, H3C 3J7

H. Nicholson, C. S. Sutton
Mount Holyoke College, South Hadley, MA 01075, USA

N. Cavallo, G. De Nardo, F. Fabozzi, C. Gatto, L. Lista, D. Piccolo, C. Sciacca
Università di Napoli Federico II, Dipartimento di Scienze Fisiche and INFN, I-80126 Napoli, Italy

M. Falbo
Northern Kentucky University, Highland Heights, KY 41076, USA

J. M. LoSecco
University of Notre Dame, Notre Dame, IN 46556, USA

J. R. G. Alsmiller, T. A. Gabriel, T. Handler
Oak Ridge National Laboratory, Oak Ridge, TN 37831, USA

F. Colecchia, F. Dal Corso, G. Michelon, M. Morandin, M. Posocco, R. Stroili, E. Torassa, C. Voci
Università di Padova, Dipartimento di Fisica and INFN, I-35131 Padova, Italy

M. Benayoun, H. Briand, J. Chauveau, P. David, C. De la Vaissière, L. Del Buono, O. Hamon, F. Le Diberder, Ph. Leruste, J. Lory, F. Martinez-Vidal, L. Roos, J. Stark, S. Versillé
Universités Paris VI et VII, Lab de Physique Nucléaire H. E., F-75252 Paris, Cedex 05, France

P. F. Manfredi, V. Re, V. Speziali
Università di Pavia, Dipartimento di Elettronica and INFN, I-27100 Pavia, Italy

E. D. Frank, L. Gladney, Q. H. Guo, J. H. Panetta
University of Pennsylvania, Philadelphia, PA 19104, USA

M. Haire, D. Judd, K. Paick, L. Turnbull, D. E. Wagoner
Prairie View A&M University, Prairie View, TX 77446, USA

J. Albert, C. Bula, M. H. Kelsey, C. Lu, K. T. McDonald, V. Miftakov, S. F. Schaffner, A. J. S. Smith, A. Tumanov, E. W. Varnes

Princeton University, Princeton, NJ 08544, USA

G. Cavoto, F. Ferrarotto, F. Ferroni, K. Fratini, E. Lamanna, E. Leonardi, M. A. Mazzoni, S. Morganti, G. Piredda, F. Safai Tehrani, M. Serra

Università di Roma La Sapienza, Dipartimento di Fisica and INFN, I-00185 Roma, Italy

R. Waldi

Universität Rostock, D-18051 Rostock, Germany

P. F. Jacques, M. Kalelkar, R. J. Plano

Rutgers University, New Brunswick, NJ 08903, USA

T. Adye, U. Egede, B. Franek, N. I. Geddes, G. P. Gopal

Rutherford Appleton Laboratory, Chilton, Didcot, Oxon., OX11 0QX, UK

N. Copty, M. V. Purohit, F. X. Yumiceva

University of South Carolina, Columbia, SC 29208, USA

I. Adam, P. L. Anthony, F. Anulli, D. Aston, K. Baird, E. Bloom, A. M. Boyarski, F. Bulos, G. Calderini, M. R. Convery, D. P. Coupal, D. H. Coward, J. Dorfan, M. Doser, W. Dunwoodie, T. Glanzman, G. L. Godfrey, P. Grosso, J. L. Hewett, T. Himel, M. E. Huffer, W. R. Innes, C. P. Jessop, P. Kim, U. Langenegger, D. W. G. S. Leith, S. Luitz, V. Luth, H. L. Lynch, G. Manzin, H. Marsiske, S. Menke, R. Messner, K. C. Moffeit, M. Morii, R. Mount, D. R. Muller, C. P. O'Grady, P. Paolucci, S. Petrak, H. Quinn, B. N. Ratcliff, S. H. Robertson, L. S. Rochester, A. Roodman, T. Schietinger, R. H. Schindler, J. Schwiening, G. Sciolla, V. V. Serbo, A. Snyder, A. Soha, S. M. Spanier, A. Stahl, D. Su, M. K. Sullivan, M. Talby, H. A. Tanaka, J. Va'vra, S. R. Wagner, A. J. R. Weinstein, W. J. Wisniewski, C. C. Young

Stanford Linear Accelerator Center, Stanford, CA 94309, USA

P. R. Burchat, C. H. Cheng, D. Kirkby, T. I. Meyer, C. Roat

Stanford University, Stanford, CA 94305-4060, USA

A. De Silva, R. Henderson

TRIUMF, Vancouver, BC, Canada V6T 2A3

W. Bugg, H. Cohn, E. Hart, A. W. Weidemann

University of Tennessee, Knoxville, TN 37996, USA

T. Benninger, J. M. Izen, I. Kitayama, X. C. Lou, M. Turcotte

University of Texas at Dallas, Richardson, TX 75083, USA

F. Bianchi, M. Bona, B. Di Girolamo, D. Gamba, A. Smol, D. Zanin

Università di Torino, Dipartimento di Fisica Sperimentale and INFN, I-10125 Torino, Italy

L. Bosisio, G. Della Ricca, L. Lanceri, A. Pompili, P. Poropat, M. Prest, E. Vallazza, G. Vuagnin

Università di Trieste, Dipartimento di Fisica and INFN, I-34127 Trieste, Italy

R. S. Panvini

Vanderbilt University, Nashville, TN 37235, USA

C. M. Brown, P. D. Jackson, R. Kowalewski, J. M. Roney
University of Victoria, Victoria, BC, Canada V8W 3P6

H. R. Band, E. Charles, S. Dasu, P. Elmer, J. R. Johnson, J. Nielsen, W. Orejudos, Y. Pan, R. Prepost, I. J. Scott, J. Walsh, S. L. Wu, Z. Yu, H. Zobernig
University of Wisconsin, Madison, WI 53706, USA

1 Introduction

The charmless hadronic decays of neutral B mesons of interest in this paper can be used to explore *CP* violation arising from two possible interference effects. Indirect *CP* violation in B^0 decays can arise from interference between the direct amplitude and one involving B^0–$\overline{B}^0$ mixing, while direct *CP* violation in charged B decays can occur via interference between tree and penguin amplitudes. The former offers the future possibility of measuring directly the CKM angle α of the Standard Model. It is expected [1] that this will require samples of order 100 million B mesons. The magnitude of direct *CP* violation is more difficult to estimate but interesting constraints can be provided with much smaller samples. In addition, the tree-penguin interference may allow measurement of the CKM angle γ [2], via measurements of the decay rates of modes presented here and the related $B \to K\pi$ and $B \to \pi\pi$ decay modes [3].

The initial challenge is to obtain significant samples of these rare decays. Many of the modes of interest have only recently been observed for the first time, or remain undiscovered [4, 5, 6]. In this paper, we describe preliminary searches of the initial *BABAR* data sample for a number of charmless hadronic B decays, and give preliminary measurements of their branching fractions. The three-body final states are limited to those with at least two charged tracks ($\pi^\pm$ or $K^\pm$) and at most one π^0. The hadronic resonances ρ and K^* are sufficiently short-lived that the modes which contain them interfere quantum mechanically with other relevant 3-body final state modes. We have however searched for them independently using appropriate kinematic selections within the Dalitz plot. The quasi-two-body decays involve an η' or ω meson accompanied by a neutral kaon or charged pion or kaon. We summarize the decay modes considered[1] as follows:

three-body	quasi-two-body
$B^+ \to K^{*0}\pi^+$	$B^+ \to \eta' K^+$
$B^+ \to \rho^0 K^+$	$B^0 \to \eta' K^0_S$
$B^+ \to K^+\pi^-\pi^+$	$B^+ \to \omega\pi^+$
$B^+ \to \rho^0\pi^+$	$B^+ \to \omega K^+$
$B^+ \to \pi^+\pi^-\pi^+$	$B^0 \to \omega K^0_S$
$B^0 \to \rho^\mp\pi^\pm$	

2 The *BABAR* detector and data

The data used in the analyses were collected with the *BABAR* detector at the PEP-II storage ring. The *BABAR* detector, described in detail elsewhere [7], consists of five active sub-detectors. Surrounding the beam-pipe is a silicon vertex tracker (SVT) to track particles of momentum less than $\sim$120 MeV/c and to provide precision measurements of the positions of charged particles of all momenta as they leave the interaction point. A beam-support tube surrounds the SVT. Outside this is a 40-layer drift chamber (DCH), filled with an 80:20 helium-isobutane gas mixture to minimize multiple scattering, providing measurements of track momenta in a 1.5 T magnetic field. It also provides dE/dx measurements to help charged particle identification. Surrounding the outer circumference of the drift chamber is a novel detector of internally reflected Cherenkov radiation (DIRC) which provides charged hadron identification in the barrel region. This consists of

[1] Charge conjugate decay modes are assumed throughout this paper.

quartz bars of refractive index ∼1.42 in which Cherenkov light is produced by relativistic charged particles. This is internally reflected and collected by an array of photomultiplier tubes, which enable Cherenkov rings to be reconstructed and associated with the charged tracks in the DCH, providing a measurement of particle velocities. Outside the DIRC is a CsI(Tl) electromagnetic calorimeter (EMC) which is used to detect photons and neutral hadrons, and to provide electron identification. The EMC is surrounded by a superconducting coil which provides the magnetic field for tracking. Outside the coil, the flux return is instrumented with resistive plate chambers (IFR), interspersed with iron which may be used for the identification of muons and K_L^0 mesons.

The data sample used for the analyses contains 8.8 million $B\overline{B}$ pairs [7], corresponding to $7.7\,\mathrm{fb}^{-1}$ taken on the $\Upsilon(4S)$ resonance. In addition, $1.2\,\mathrm{fb}^{-1}$ of data taken off-resonance have been used to validate the contribution to backgrounds resulting from e^+e^- annihilation into light $q\overline{q}$ pairs. These data have all been processed with reconstruction software to determine the three-momenta and positions of charged tracks and the energies and positions of photons and merged π^0 s. Refined information on particle type from the various sub-detectors described above is also provided, and is used in particle identification algorithms in the analyses, as described below.

3 Candidate selection

Charged tracks are required to satisfy some standard track criteria, including a requirement that the momentum is less than $10\,\mathrm{GeV}/c$ and that the transverse momentum is greater than $0.1\,\mathrm{GeV}/c$. They are required to have at least 20 hits in the DCH and to originate close to the beam-spot.

Photon candidates are identified in our calorimeter as deposits of energy unassociated with charged tracks. Resolved π^0 s are reconstructed by combining pairs of photon candidates and requiring that the invariant mass of the resultant candidate is between $100\,\mathrm{MeV}/c^2$ and $170\,\mathrm{MeV}/c^2$. Photon candidates used in π^0 reconstruction are required to have a minimum energy of 50 MeV. In addition to resolved π^0 s, unresolved π^0 s are identified as single clusters of energy deposited in the EMC without distinct local maxima and satisfying certain topological criteria [7]. For the final event selection, we tighten the requirement on the π^0 mass to between $120\,\mathrm{MeV}/c^2$ and $150\,\mathrm{MeV}/c^2$.

Neutral kaons are reconstructed through the decay $K_S^0 \to \pi^+\pi^-$. K_S^0 candidates are formed from combinations of two oppositely charged tracks satisfying basic track criteria similar to those mentioned above, except with a looser constraint on their proximity to the beam spot. We require that the K_S^0 candidate's flight length exceed 2 mm, the angle between its flight and momentum directions be less than 40 mr, and the mass lie within $\pm 10\,\mathrm{MeV}/c^2$ of nominal.

We reconstruct ω mesons using the dominant decay channel, $\omega \to \pi^-\pi^+\pi^0$, which has a branching fraction of 88.8%. Candidates are obtained as combinations of two charged tracks with opposite signs and one π^0 candidate. The invariant mass of the ω candidate is required to be within $0.05\,\mathrm{GeV}/c^2$ of the known ω mass [6]. Figure 1 shows the $\pi^-\pi^+\pi^0$ invariant mass for ω candidates with a center-of-mass momentum between 1.9 and $3.1\,\mathrm{GeV}/c$. The signal is fitted with a Breit-Wigner function with the natural width of the ω ($8.4\,\mathrm{MeV}/c^2$) convoluted with a Gaussian resolution function, and the combinatorial background is fitted with a second-order polynomial. The Gaussian resolution function is found to have a width of $8\,\mathrm{MeV}/c^2$.

Candidate ρ and K^* mesons are reconstructed by combining pairs of appropriately charged tracks and/or π^0 candidates, with the assumption of the relevant final-state rest masses, and requiring that the combination have an invariant mass sufficiently close to the known resonance mass. Requirements for the invariant masses are analysis-dependent, and are described below.

The η meson is reconstructed by combining pairs of photon candidates with a minimum energy

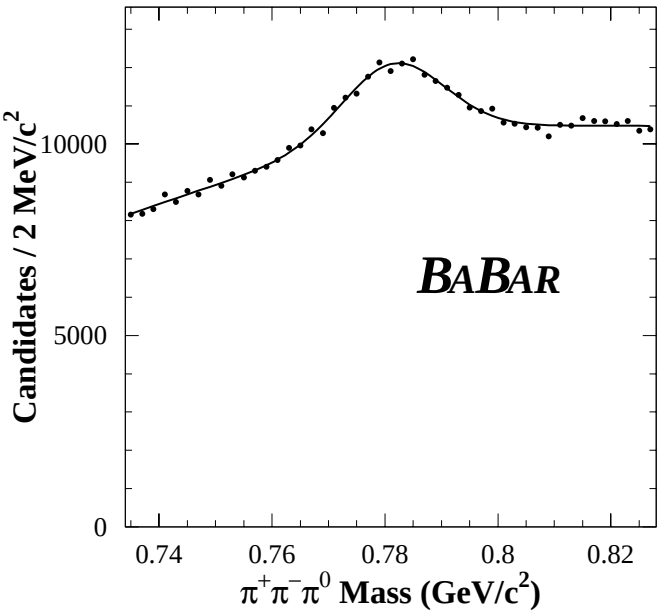

Figure 1: Mass spectrum of hard ω candidates in on-resonance data, fitted with a Breit-Wigner convoluted with a Gaussian for the signal and a second-order polynomial for the background.

of 50 MeV. The reconstructed η mass for data is shown in Fig. 2. We obtain a width of 19 MeV/c^2 for a Gaussian fit, with the background described by a second-order polynomial. The η' meson is reconstructed in the $\eta' \to \eta\pi^+\pi^-$ decay mode. This is done by combining η candidates with pairs of oppositely charged tracks. A mass constraint is used to improve the η mass resolution. Fig. 2 shows the invariant mass distribution for all $\eta\pi\pi$ candidates with momentum above 2 GeV/c. From a fit to the sum of a Gaussian and a second-order polynomial, we obtain a width of 4.7 MeV/c^2 for the η' peak.

For B decays to final states formed from a pseudoscalar and a vector meson, the vector meson is polarized. We make use of the angular distribution of the vector meson decay products to distinguish between signal and background. We compute in the rest frame of the vector meson the cosine of the angle θ_H between the direction of one of the vector meson daughters (the normal to the decay plane in the case of the ω) and the direction of the B meson in the same frame. We expect signal events to be distributed according to $\cos^2\theta_H$, while background should be approximately flat.

To veto electrons, we require that charged hadrons satisfy $E/p < 0.9$, where E is the energy measured in the calorimeter associated with a charged track of momentum p. We also require that kaons be positively identified as such with a combination of the information from the DIRC and the drift chamber $\mathrm{d}E/\mathrm{d}x$. For pions, we simply require that they not be identified as kaons.

Reconstruction of B candidates is done by forming all combinations of the appropriate final-state candidate particles, and requiring them to satisfy kinematic constraints appropriate for B mesons. We use two kinematic variables [7] for this: $m_{\rm ES} = \sqrt{(\frac{1}{2}s + \mathbf{p}_0\cdot\mathbf{p}_B)^2/E_0^2 - p_B^2}$, where the subscripts 0 and B refer to the e^+e^- system and the B candidate, respectively; and $\Delta E = E_B^* - \sqrt{s}/2$, where

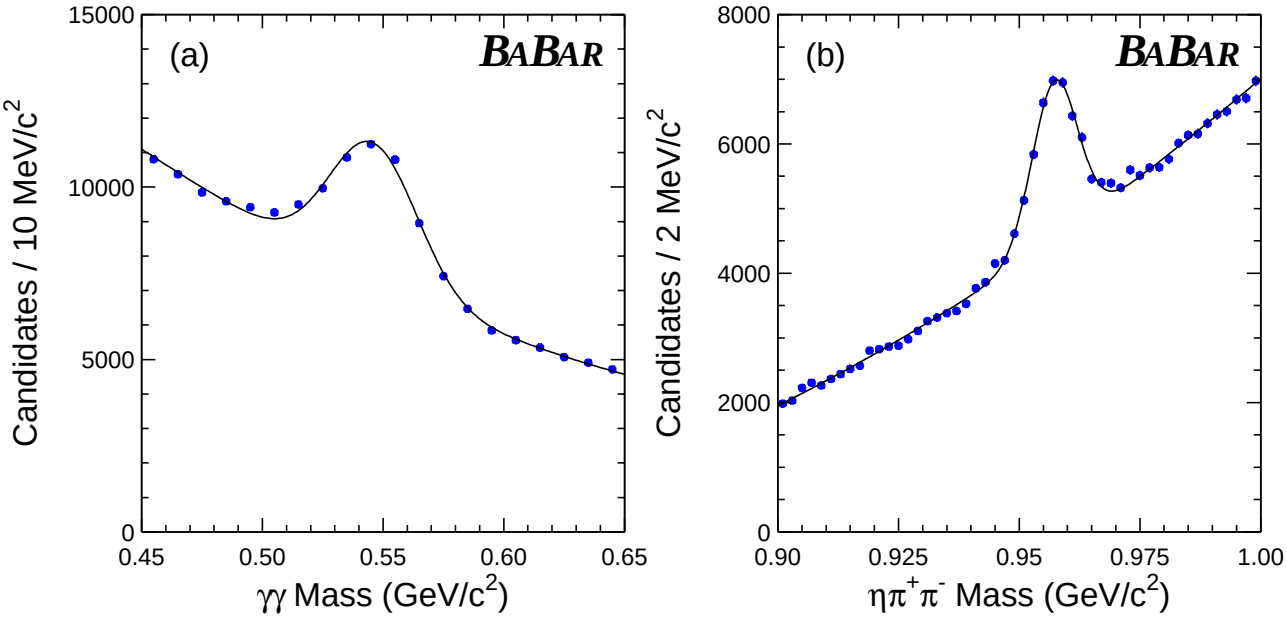

Figure 2: Distribution of (a) $\gamma\gamma$ ($\sigma = 19$ MeV/c^2) mass, and (b) $\eta\pi^+\pi^-$ ($\sigma = 4.7$ MeV/c^2) mass in on-resonance data.

E_B^* is the B candidate energy in the center-of-mass frame. For signal events, the former has a value close to the B meson mass [2] and the latter should be close to zero. In our analyses, the appropriate final state masses are assigned to the final state particles in calculating ΔE.

We have measured the expected distributions of the signal with respect to $m_{\rm ES}$ and ΔE, using two calibration modes described in Section 4. Based on these, we define a "signal region" in the $m_{\rm ES}$–ΔE plane by $|m_{\rm ES} - \langle m_{\rm ES}\rangle| < 6\,{\rm MeV}/c^2$ and $|\Delta E - \langle \Delta E\rangle| < 70\,{\rm MeV}$, where $\langle m_{\rm ES}\rangle$ and $\langle \Delta E\rangle$ indicate the mean values obtained in the calibration modes. This signal region is common to all modes, except $B^+ \to \omega h^+$ (see Section 6.2).

4 Calibration with charmed B decays

The decay mode $B^+ \to \overline{D}{}^0\pi^+$, $\overline{D}{}^0 \to K^+\pi^-$ results in a final state containing three charged tracks, while the same B^+ decay with $\overline{D}{}^0 \to K^+\pi^-\pi^0$ yields in addition a π^0. The D^0 mass is small compared to that of the B, so that this decay has kinematics similar to charmless B decays to two

[2] A nearly equivalent constrained mass that we use for some of the modes is $m_{\rm EC} = \sqrt{{E_B^*}^2 - {p_B^*}^2}$, obtained from a fit constrained by $E_B^* = \frac{1}{2}\sqrt{s}$.

light mesons such as $B \to \rho\pi$, $B \to K^*\pi$ or $B \to \omega\pi$. The product branching fractions are known to about 10% precision and are roughly an order of magnitude larger than those expected of many charmless modes. A study of these decays can therefore be used to calibrate the variables used in the charmless analyses. The most significant difference is that the D^0 has a measurable lifetime, resulting in decay tracks which do not share a common vertex with the pion from the B decay.

The candidate selection proceeds along similar lines to those described earlier for the charmless decay modes, except that the invariant mass of the D^0 daughters, assumed to be $\pi K(\pi^0)$, must be consistent with the D^0 mass. The background is estimated by counting events in a "sideband" of the $m_{\rm ES}$–ΔE distribution, and also by looking at $K\pi\pi(\pi^0)$ track combinations which satisfy the selection criteria but which have an incorrect charge combination (the kaon charge is opposite to that of the B meson). The extrapolation from sideband to signal region is done in the same way as described for the charmless analyses.

The efficiency of the selection for $B^+ \to \overline{D}^0\pi^+, \overline{D}^0 \to K^+\pi^-[\pi^0]$ is $(23 \pm 2)\%$ $[(12 \pm 1)\%]$, evaluated as described in Section 6. When combined with the total number of B decays the product branching fraction for $B^+ \to \overline{D}^0\pi^+, \overline{D}^0 \to K^+\pi^-[\pi^0]$ is measured to be $(2.21 \pm 0.11) \times 10^{-4}$ $[(6.79 \pm 0.32) \times 10^{-4}]$, where the errors are statistical only. These are both consistent with the corresponding world-average values [6].

The selected signals in these modes have been used to estimate the $m_{\rm ES}$ and ΔE resolution functions of our target modes in data. We find the $m_{\rm ES}$ resolution to be 2.7 ± 0.1 MeV/c^2 in the mode with only three charged tracks and 3.0 ± 0.1 MeV/c^2 in the mode with a π^0. The corresponding ΔE resolutions are 26 ± 2 MeV in the mode with only three charged tracks and 33 ± 2 MeV in the mode with a π^0. The measured values were used to inform the choice of signal region, noted at the end of Section 3 and for calculation of the selection efficiency and its uncertainty.

5 Background characterization and suppression

Charmless hadronic modes suffer very large amounts of background from random combinations of tracks, mostly from light quark and charm continuum production. Such backgrounds may be reduced by selection requirements on the event topologies computed in the $\Upsilon(4S)$ rest frame. We use the angle θ_T between the thrust axis of the B meson decay and the thrust axis of the rest of the event. For continuum-related backgrounds, these two directions tend to be aligned because the reconstructed B candidate daughters generally lie in the same jets as those in the rest of the event. By contrast, in B events, the decay products from one B meson are independent of those in the other, making the distribution of this angle isotropic. In consequence, requiring that this opening angle be significant provides a strong suppression of continuum backgrounds.

Other event shape variables also help to separate signal and background. We combine several variables in a Fisher discriminant $\mathcal{F}$ [8]. The variables contained in $\mathcal{F}$ are:

- The summed energy in nine annular cones of angular extent 175 mrad, coaxial with the thrust axis of the B candidate.
- The absolute value of the cosine of the angle between the B direction and the beam axis.
- The absolute value of the cosine of the angle between the thrust axis of the B candidate and the beam axis.

The Fisher discriminant is a linear combination of these 11 variables. The coefficients for each variable are chosen to maximize the separation between training samples of signal and background

events. These coefficients were determined for the $B^+ \to \omega h^+$ analysis and the same coefficients are used for the other ω and η' analyses.

Despite the power of such topological variables to reduce the combinatorial backgrounds, most of the modes we have searched for continue to suffer significant background levels. Even after stringent selection criteria have been applied, it is necessary to do a background subtraction to isolate a signal or set an upper limit. In order to do this, the background in the signal region must be estimated. This is done by noting that the amount of background in the signal region should be related to the amount in a sideband region, located near the signal region in the $m_{\rm ES}$-ΔE plane. We define $\mathcal{A}$, to be the ratio of the number of candidates in the signal region to the number in the sideband region. Two different methods have been used to estimate $\mathcal{A}$. In the first, the shape of the distribution of the background as a function of $m_{\rm ES}$ is measured from on-resonance data. This is done with events slightly displaced from the signal region in the ΔE variable ($0.1 < |\Delta E\,| < 0.3$). In the second method, off-resonance data are used, simply counting the numbers of candidates in the signal and sideband regions to provide the ratio. The first method is used in the three-body measurements, and the second method in the quasi-two-body measurements. In each case, the alternative method has been used to evaluate systematic errors. Where insufficient data are available for the off-resonance studies, selection criteria in uncorrelated variables have been loosened, to provide additional statistics in the determination of $\mathcal{A}$. We find that the value of $\mathcal{A}$ is quite independent of the decay mode provided the selection criteria are common. For some modes with limited statistics we substitute a more precise value of $\mathcal{A}$ from a mode in which it is better measured. Simulated light-quark (u, d, s, c) continuum events are used to check the value of $\mathcal{A}$ and provide a statistically-independent sample for optimization of event selections in the final stage of the analysis.

6 Analysis

The branching fractions are calculated according to

$$\mathcal{B} = \frac{N_1 - \mathcal{A}N_2}{N_{B\overline{B}} \times \epsilon} \tag{1}$$

where N_1 is the number of candidates in the signal region for on-resonance data; N_2 is the number of candidates in on-resonance data observed in the sideband region, so that $\mathcal{A}N_2$ is the estimated number of background candidates in the signal region; $N_{B\overline{B}}$ is the number of $B\overline{B}$ pairs produced and ϵ is the signal efficiency. Except in particular cases, explained below, the sideband is specified by $5.20 < m_{\rm ES} < 5.27\,{\rm GeV}/c^2$, $|\Delta E - \langle\Delta E\rangle\,| < 0.2\,{\rm GeV}$, where $\langle\Delta E\rangle$ was defined in Section 3.

The numbers and distributions of candidates within the signal region remain unknown to us until all aspects of the analysis are finalized. The final selection criteria are chosen to maximize the sensitivity of the signal, defined as the expected signal yield divided by its statistical uncertainty. Once chosen, neither the background description nor the cuts are changed. This procedure has been followed independently for each channel.

For the signal efficiency in Eq. (1), we use simulated signal events and the same selection criteria as used for the data. The efficiencies due to tracking, particle identification and the ΔE and $m_{\rm ES}$ selection criteria are determined from independent control samples from the data.

6.1 Modes with three-body final states

The selection criteria which are varied during optimization are the thrust-angle requirement, the helicity-angle requirement and the mass requirement on resonance candidates. In addition to these and the selection criteria described in Section 3, a quality requirement of $\chi^2 < 20$ is applied to the three (two) charged track vertices in all charged (neutral) three-body analyses. Finally, a veto on all pairs of tracks which are consistent with the $\overline{D}^0 \to K^+\pi^-$ decay hypothesis (independent of particle identification) is applied in all three-body analyses. This has no significant effect on our results in any mode except $B^+ \to \rho^0 K^+$. The results for these analyses are summarized in Table 1. The branching fraction central values are calculated from Eq. 1. The significance values given are the probabilities of a fluctuation of the background to account for the observed yield, in equivalent Gaussian standard deviations.

The background extrapolation is validated, albeit with low statistics, by the observed ratios of events in signal and sideband regions in off-resonance data. In each case, we found that the number of events falling in the signal region was consistent within one standard deviation with the expectation from the sideband regions.

The $B^+ \to \rho^0 K^+$ mode has the additional complication of cross-talk background from the $B^+ \to \eta' K^+$ mode with $\eta' \to \rho^0\gamma$. The γ can be quite soft and in such cases the ρ^0 and K^+ may imitate the $B^+ \to \rho^0 K^+$ signal. We correct for this by processing simulated events from this background mode using the full set of optimized selection criteria for the $B^+ \to \rho^0 K^+$ mode. We obtain an efficiency for this mode of 2.4%, leading to a reduction of the observed branching fraction by 2.0×10^{-6}. The existence of this B-related background was foreseen, and for this reason the sideband used to estimate the background is somewhat smaller than that used for the other modes, to ensure that there was no significant leakage of this background into the light-quark background estimate. Cross-talk among the other modes considered is found from Monte Carlo simulation to be negligible at the current level of precision.

The distributions of $m_{\rm ES}$ and ΔE for the resonant three-body modes are shown in Fig. 3.

We note that the analyses of the two modes $B^+ \to K^+\pi^-\pi^+$ and $B^+ \to \pi^+\pi^-\pi^+$ differ in some respects from those with a resonance. We remove all two-body combinations with invariant masses less than 2 GeV/c^2, and in addition veto combinations of tracks consistent with the decay mode $B^+ \to J/\psi\, K^+$. The distributions of $m_{\rm ES}$ and ΔE for the non-resonant modes are shown in Fig. 4.

6.2 Modes with ω and η'

We summarize the results of the measurements in Table 2. For all decay modes, we require $|\cos\theta_T| < 0.9$, and then find the optimum selection requirement in $\mathcal{F}$. The latter is listed for each mode in the table. Also listed are the selection criteria on resonance masses and π^0 or η masses. The selection criteria are centered on the known masses [6]. We also require that $|\cos\theta_H|$ be greater than 0.55 (0.4) for the decay modes $B^+ \to \omega h^+ (B^0 \to \omega K^0)$.

Table 2 gives the yields in the signal and sideband regions, both for on- and off-resonance data. The signal region is defined as $|m_{\rm ES} - 5.279| < 0.006$ GeV/c^2 and $|\Delta E| < 0.070$ GeV, except for $B^+ \to \omega h^+$ where we use $-0.113 < \Delta E < 0.070$ GeV, allowing for the 43 MeV shift of $B^+ \to \omega K^+$ when the energy of the K^+ is computed with a pion mass. The sideband is defined as $5.20 < m_{\rm ES} < 5.27$ GeV/c^2 and $|\Delta E| < 0.2$ GeV. The branching fraction central values and significance values are calculated in the same way as for Table 1.

In Fig. 5 we illustrate the reconstruction of the $B^+ \to \eta' K^+$ states with plots of the kinematic

Table 1: Results for the three-body final state analyses. Energies and masses are in units of MeV. See the text for an explanation of the quantities given.

Quantity	$B^+ \to K^{*0}\pi^+$	$B^+ \to \rho^0 K^+$	$B^+ \to K^+\pi^-\pi^+$	$B^+ \to \rho^0\pi^+$	$B^+ \to \pi^+\pi^-\pi^+$	$B^0 \to \rho^\mp\pi^\pm$
$\cos\theta_T$	0.70	0.60	0.70	0.55	0.70	0.50
K^{*0}/ρ mass	± 100	± 200	N/A	± 200	N/A	± 150
K^{*0}/ρ helicity angle	0.40	0.40	N/A	0.40	N/A	0.30
Signal events						
On-res data	22	25	33	64	32	77
Off-res data	1	1	3	4	5	6
Sideband events						
On-res data	319	256	454	1057	722	1129
Off-res data	50	45	60	166	92	183
$\mathcal{A}$	0.037	0.056	0.037	0.037	0.037	0.037
Est. BG	11.8 ± 0.9	14.3 ± 1.2	16.7 ± 1.1	39.1 ± 1.9	26.6 ± 1.4	41.5 ± 4.3
Signal	10.2 ± 4.8	10.7 ± 5.1	16.3 ± 5.8	24.9 ± 8.2	5.4 ± 5.7	35.5 ± 9.8
$\epsilon \times$ secondary $\mathcal{B}_i$ (%)	9.7 ± 0.9	9.8 ± 1.0	6.0 ± 0.6	11.9 ± 1.2	8.2 ± 0.8	$8.3^{+1.0}_{-1.1}$
Stat. sign. (σ)	2.4	2.2	3.2	3.3	0.7	4.5
cross-talk correction ($\times 10^{-6}$)		-2.0				
$\mathcal{B}(\times 10^{-6})$	$13 \pm 6 \pm 1$	$10 \pm 6 \pm 2$	$31 \pm 11 \pm 3$	$24 \pm 8 \pm 3$	$7.5^{+7.9}_{-7.5} \pm 0.8$	$49 \pm 13^{+6}_{-5}$
90% CL limit	< 28	< 29	< 54	< 39	< 22	

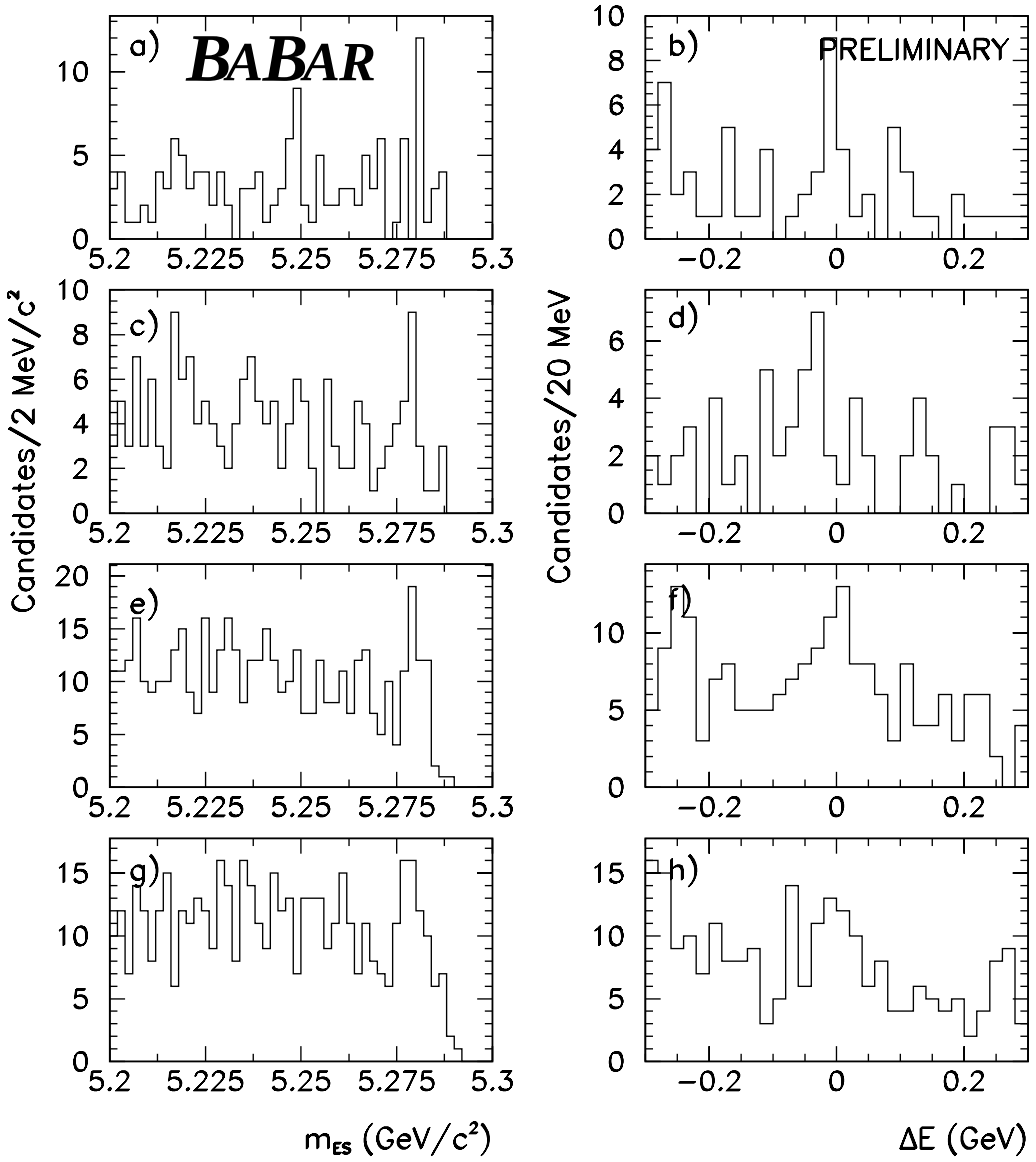

Figure 3: Distributions in $m_{\rm ES}$ and ΔE after all other selection criteria have been applied for (a, b) $B^+ \to K^{*0}\pi^+$, (c, d) $B^+ \to \rho^0 K^+$, (e, f) $B^+ \to \rho^0\pi^+$, (g, h) $B^0 \to \rho^{\mp}\pi^{\pm}$.

Table 2: Results for the quasi-two-body decay analyses. Energies and masses are in units of MeV. See the text for an explanation of the quantities given.

Quantity	$B^+ \to \omega h^+$	$B^0 \to \omega K^0$	$B^+ \to \eta' K^+$	$B^0 \to \eta' K^0$
$\mathcal{F}$	-0.4	-0.2	0.3	0.6
ω/η' mass	± 20	± 20	± 10	± 10
π^0/η mass	± 15	± 15	± 45	± 10
Signal events				
On-res data	13	0	14	2
Off-res data	1	0	0	0
Sideband events				
On-res data	128	19	45	14
Off-res data	16	6	8	1
$\mathcal{A}$	0.055	0.042	0.042	0.042
Est. BG	7.1 ± 0.9	0.8 ± 0.2	1.9 ± 0.3	0.6 ± 0.2
Signal	5.9 ± 3.6	-0.8 ± 0.0	12.1 ± 3.7	1.4 ± 1.4
Eff. ϵ (%)	8.5	7.6	17.1	10.0
Secondary $\mathcal{B}$ (%)	88.8	30.5	17.2	6.0
$\epsilon \times$ secondary $\mathcal{B}$ (%)	7.5 ± 1.4	2.3 ± 0.4	2.9 ± 0.4	0.60 ± 0.09
Stat. sign. (σ)	1.7	0.0	5.3	1.1
$\mathcal{B}(\times 10^{-6})$	$8.9 \pm 5.4 \pm 2.2$	0.0	$62 \pm 18 \pm 8$	$27 \pm 27 \pm 5$
90% CL limit	< 24	< 14		< 112

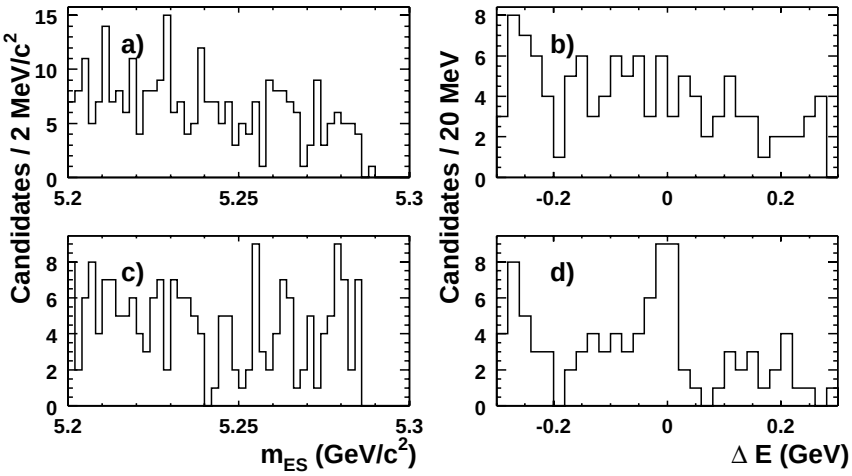

Figure 4: $m_{\rm ES}$ and ΔE distributions for (a, b) $B^+ \to \pi^+\pi^-\pi^+$ and (c, d) $B^+ \to K^+\pi^-\pi^+$ non-resonant analyses after the final selection.

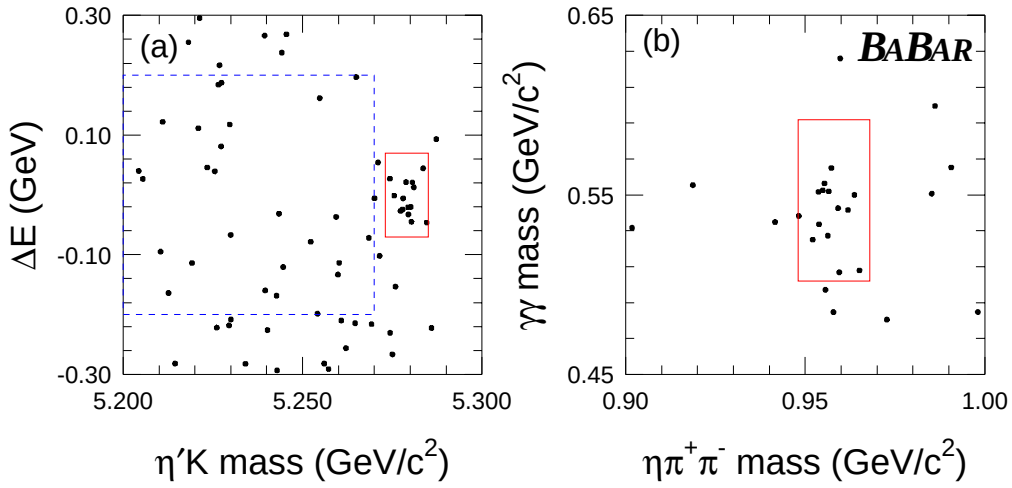

Figure 5: Kinematics of $B^+ \to \eta' K^+$, $\eta' \to \eta\pi^+\pi^-$: (a) ΔE vs. $m_{\rm ES}$ and (b) $\gamma\gamma$ vs. $\eta\pi^+\pi^-$ invariant mass.

variables associated with the B meson and daughter resonance. For the other decay modes we report our final results as 90% confidence upper limits.

The distributions for all decay modes, projected on to the $m_{\rm ES}$ and ΔE axes, are presented in Fig. 6.

7 Systematic errors

The primary uncertainty in the signal yield is the counting statistics of the accepted events in the signal region. The systematic uncertainty on the background estimate receives contributions from the number of events observed in the on-resonance sideband region and from the ratio $\mathcal{A}$. The

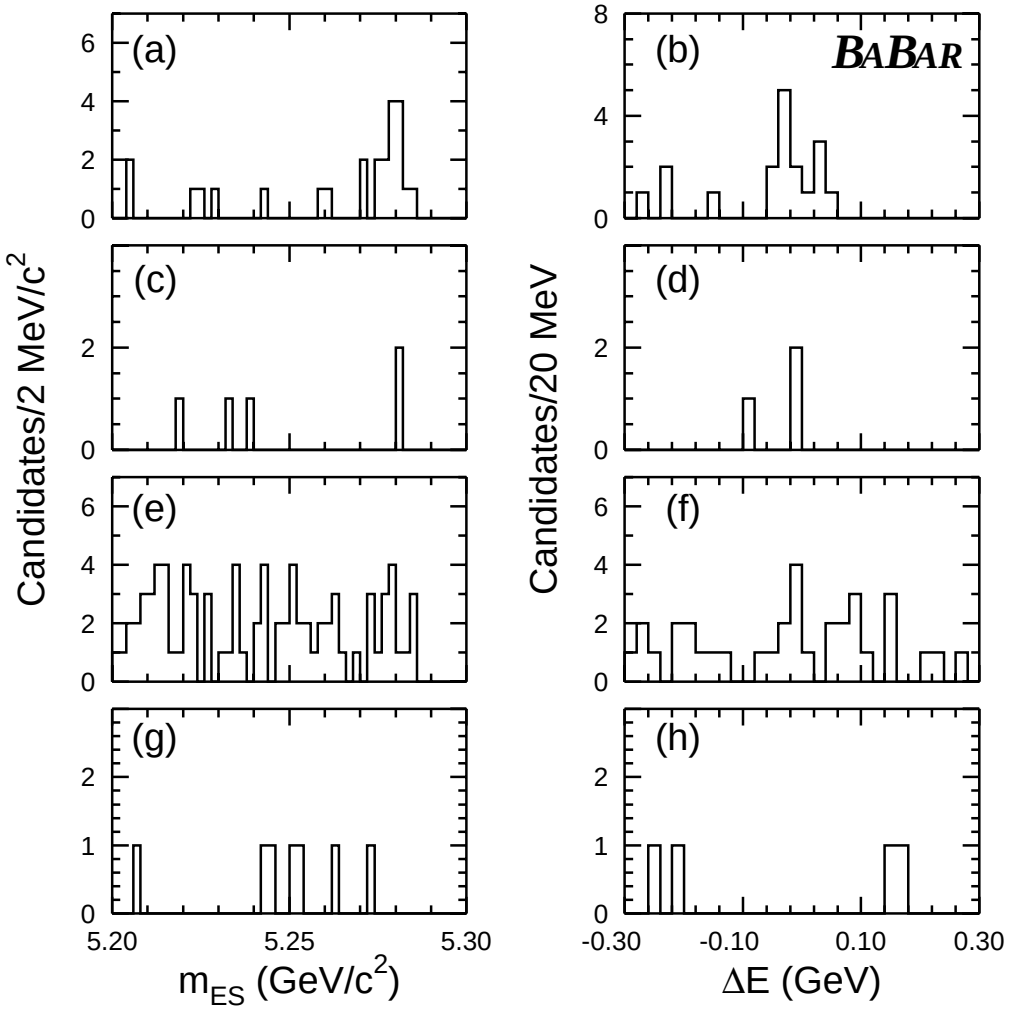

Figure 6: Distributions in $m_{\rm ES}$ and ΔE after all other selection criteria have been applied for (a, b) $B^+ \to \eta' K^+$, (c, d) $B^0 \to \eta' K^0$, (e, f) $B^+ \to \omega h^+$, (g, h) $B^0 \to \omega K^0$.

uncertainty on the latter depends on the statistics of the off-resonance samples and on the method used to determine it. We estimate an overall uncertainty in $\mathcal{A}$ of 4% for the charged three-body modes and 10% for the other modes.

The branching fraction itself has a multiplicative uncertainty from our knowledge of the efficiency, ϵ. We measure ϵ using signal Monte Carlo simulation, and a significant uncertainty arises from limited signal mode statistics, the fractional error due to the size of the Monte Carlo samples used to estimate ϵ varies between 4% and 7%, depending on the mode. The accuracy of the simulation is subject to systematic uncertainties in the efficiency of tracking and calorimetric shower detection, particle identification criteria, and the resolutions on quantities used to define selection criteria. At present the dominant uncertainties are in the tracking, π^0/η reconstruction, and Fisher Discriminant selection efficiency, with some variation on their relative importance depending on the decay mode.

Independent studies determine an absolute track-finding efficiency uncertainty of 2.5% per track, added coherently for all tracks required in the analyses. For π^0 or η reconstruction, we assign an uncertainty of 5%, and add an additional uncertainty of 1-5% in quadrature to account for the effect of the final mass requirement. For the Fisher Discriminant selection, the uncertainty on the efficiency can vary considerably, depending on the tightness of the selection requirement. The uncertainty ranges from only a few percent for decay modes with low background, to as much as 15% for ones which need a tight selection requirement. The number of produced $B\overline{B}$ events has been estimated in separate studies [7] with an estimated uncertainty of 3.6%. Uncertainties in the particle identification and $m_{\rm ES}$ and ΔE selection criteria contribute systematic uncertainties of 2-4%, depending on mode. The overall systematic uncertainty is the quadrature sum of the contributions from all sources.

For modes in which we find an upper limit for the branching fraction, we account for the uncertainty of the efficiency by using in Eq. 1 the measured efficiency reduced by one standard deviation in the systematic error.

8 Summary

We have presented a number of preliminary measurements of charmless hadronic B decays, summarized in Table 3. We observe significant signals for $B^+ \to \eta' K^+$ and $B^0 \to \rho^\mp \pi^\pm$, with branching fractions $\mathcal{B}(B^+ \to \eta' K^+) = (62 \pm 18 \pm 8) \times 10^{-6}$ and $\mathcal{B}(B^0 \to \rho^\mp \pi^\pm) = (49 \pm 13^{+6}_{-5}) \times 10^{-6}$. Upper limits are given for the remaining channels we have studied. In each case, our determinations are consistent with earlier published measurements [4, 5, 6].

Acknowledgments

We are grateful for the contributions of our PEP-II colleagues in achieving the excellent luminosity and machine conditions that have made this work possible. We acknowledge support from the Natural Sciences and Engineering Research Council (Canada), Institute of High Energy Physics (China), Commissariat à l'Energie Atomique and Institut National de Physique Nucléaire et de Physique des Particules (France), Bundesministerium für Bildung und Forschung (Germany), Istituto Nazionale di Fisica Nucleare (Italy), The Research Council of Norway, Ministry of Science and Technology of the Russian Federation, Particle Physics and Astronomy Research Council (United

Table 3: Summary of branching fraction measurements. Inequality denotes 90% CL upper limit, including systematic uncertainties.

Decay mode	$\mathcal{B}(\times 10^{-6})$
$B^+ \to K^{*0}\pi^+$	< 28
$B^+ \to \rho^0 K^+$	< 29
$B^+ \to K^+\pi^-\pi^+$	< 54
$B^+ \to \rho^0\pi^+$	< 39
$B^+ \to \pi^+\pi^-\pi^+$	< 22
$B^0 \to \rho^\mp\pi^\pm$	$49 \pm 13^{+6}_{-5}$
$B^+ \to \eta' K^+$	$62 \pm 18 \pm 8$
$B^0 \to \eta' K^0$	< 112
$B^+ \to \omega h^+$	< 24
$B^0 \to \omega K^0$	< 14

Kingdom), the Department of Energy (US), and the National Science Foundation (US). In addition, individual support has been received from the Swiss National Foundation, the A. P. Sloan Foundation, the Research Corporation, and the Alexander von Humboldt Foundation. The visiting groups wish to thank SLAC for the support and kind hospitality extended to them.

References

[1] P. F. Harrison and H. R. Quinn, eds., "The *BABAR* physics book", SLAC-R-405 (1998).

[2] M. Neubert and J. Rosner, Phys. Lett. **B441**, 403 (1998); M. Neubert, JHEP **9902**, 14 (1999); X. G. He, W. S. Hou and K. C. Yang, Phys. Rev. Lett. **83**, 1100 (1999).

[3] *BABAR* Collaboration, B. Aubert *et al.*, "Measurement of branching fractions for two-body charmless B decays to charged pions and kaons at *BABAR*", *BABAR*-CONF-00/14, submitted to the XXXth International Conference on High Energy Physics, Osaka, Japan.

[4] CLEO Collaboration, C. P. Jessop *et al.*, CLNS 99/1652, CLEO 99-19, (2000).

[5] CLEO Collaboration, S. J. Richichi *et al.*, Phys. Rev. Lett. **85**, 520 (2000).

[6] Particle Data Group, D.E. Groom *et al.*, Eur. Phys. Jour. C **15**, 1 (2000).

[7] *BABAR* Collaboration, B. Aubert *et al.*, "The first year of the *BABAR* experiment at PEP-II", *BABAR*-CONF-00/17, submitted to the XXXth International Conference on High Energy Physics, Osaka, Japan.

[8] CLEO Collaboration, D. M. Asner *et al.*, Phys. Rev. **D53**, 1039 (1996).